OXFORD

Human Molecular Genetics, 2015, Vol. 24, No. 15 4225–4237

doi: 10.1093/hmg/ddv155
Advance Access Publication Date: 1 May 2015
Original Article

ORIGINAL ARTICLE

How much dystrophin is enough: the physiological consequences of different levels of dystrophin in the *mdx* mouse

Caroline Godfrey[1,†], Sofia Muses[2,†], Graham McClorey[1], Kim E. Wells[2], Thibault Coursindel[3,4], Rebecca L. Terry[2], Corinne Betts[1], Suzan Hammond[1], Liz O'Donovan[3], John Hildyard[2], Samir El Andaloussi[1,5], Michael J. Gait[3], Matthew J. Wood[1,‡] and Dominic J. Wells[2,‡,*]

[1]Department of Physiology, Anatomy and Genetics, University of Oxford, South Parks Road, Oxford OX1 3QX, UK, [2]Department of Comparative Biomedical Sciences, Royal Veterinary College, Royal College Street, London NW1 0TU, UK, [3]Medical Research Council, Laboratory of Molecular Biology, Francis Crick Avenue, Cambridge CB2 0QH, UK, [4]GENEPEP SA, Les Coteaux St Roch, 12 Rue du Fer à Cheval, 34430 St Jean de Védas, France and [5]Department of Laboratory Medicine, Karolinska Institutet, Hälsov. 7, SE-14186 Huddinge, Sweden

*To whom correspondence should be addressed. Tel: +44 2032148024; Email: dwells@rvc.ac.uk

Abstract

Splice modulation therapy has shown great clinical promise in Duchenne muscular dystrophy, resulting in the production of dystrophin protein. Despite this, the relationship between restoring dystrophin to established dystrophic muscle and its ability to induce clinically relevant changes in muscle function is poorly understood. In order to robustly evaluate functional improvement, we used *in situ* protocols in the *mdx* mouse to measure muscle strength and resistance to eccentric contraction-induced damage. Here, we modelled the treatment of muscle with pre-existing dystrophic pathology using antisense oligonucleotides conjugated to a cell-penetrating peptide. We reveal that 15% homogeneous dystrophin expression is sufficient to protect against eccentric contraction-induced injury. In addition, we demonstrate a >40% increase in specific isometric force following repeated administrations. Strikingly, we show that changes in muscle strength are proportional to dystrophin expression levels. These data define the dystrophin restoration levels required to slow down or prevent disease progression and improve overall muscle function once a dystrophic environment has been established in the *mdx* mouse model.

Introduction

The application of antisense oligonucleotide (AO)-based methods to modulate pre-mRNA splicing in Duchenne muscular dystrophy (DMD, OMIM #310200) has placed this monogenic disorder at the forefront of advances in gene therapy. The majority of mutations underlying DMD are genomic deletions encompassing multiple exons which lead to a disruption of the open reading frame and result in an absence of the essential protein dystrophin. Dystrophin deficiency causes progressive muscle degeneration and wasting followed by the emergence of respiratory and cardiac complications and ultimately premature death (1). Antisense oligonucleotides can be used for targeted exon exclusion

† The authors wish it to be known that, in their opinion, the first two authors should be regarded as joint First (co-responding) Authors, respectively.
‡ The authors wish it to be known that, in their opinion, the last two authors should be regarded as joint Last (co-responding) Authors, respectively.
Received: January 26, 2015. **Revised:** March 31, 2015. **Accepted:** April 27, 2015

© The Author 2015. Published by Oxford University Press. All rights reserved. For Permissions, please email: journals.permissions@oup.com

resulting in the correction of aberrant reading frames and the production of an internally deleted, yet largely functional, dystrophin protein (2).

Although the production of dystrophin using AO therapy has been demonstrated in clinical trials (3–6), the level of internally truncated protein required to provide meaningful clinical improvement in DMD patients is unclear (7). Studies of patient cohorts with the allelic yet comparatively milder disorders of Becker muscular dystrophy [OMIM 300376] and X-linked cardiomyopathy [OMIM 302045] indicate that sarcolemmal levels of dystrophin as low as 30% are sufficient to avert the onset of symptomatic skeletal muscle degeneration (8,9).

Dystrophin restoration levels reported following systemic clinical trials with repeated administrations of both phosphorodiamidate morpholino oligomer (PMO) and 2′-O-methyl chemistries were highly variable (3,4). Although dystrophin levels of up to 23% of normal levels were observed (quantified on western blot), the lack of pre-treatment biopsies in one trial (4), the uneven distribution of dystrophin between muscle fibers, along with the limited number of patients, has largely hampered the assessment of the relationship between the levels of dystrophin achieved and functional muscle improvements.

Varying degrees of disease amelioration have been demonstrated using transgenic mouse models constitutively expressing a range of dystrophin protein levels; with levels approaching 20% preventing the development of dystrophic symptoms, whereas some improvements in muscle function and survival have been reported from as low as 4% (10–14). While correlating dystrophin levels from mouse models and patient cohorts has provided vital information on the levels of dystrophin needed to prevent the onset of severe pathology, further work is needed to establish the minimal levels of dystrophin required to reduce pathology and improve muscle function once a dystrophic environment has been established.

The *mdx* mouse is widely used as a pre-clinical model for DMD. The mouse strain does not exhibit any pathology until ~3 weeks of age when the muscle starts to undergo cycles of severe skeletal muscle degeneration and regeneration. Muscle pathology is marked until 8–10 weeks of age, before stabilizing to a relatively low but constant level of muscle necrosis and regeneration throughout the life-span of the mouse (15–18). Typically pre-clinical AO therapies developed in the *mdx* mouse have commenced during this initial period (<10 weeks of age) providing a useful model for assessing any delay in the onset of necrosis and they allow appreciable differences in pathology to be readily identified. However, in most, if not all, patients there will be an established dystrophic environment prior to the initiation of therapy.

We set out to evaluate the minimum levels of dystrophin needed to reduce myopathic pathophysiology in an established dystrophic environment. In order to investigate this in detail, we assessed changes in muscle following treatment of the *mdx* mouse model using a PMO-based AO to skip *Dmd* exon 23. We enhanced the delivery of the PMO using a highly efficacious peptide, Pip6a, conjugated to the PMO (Pip6a-PMO) (19). Treatment in all cases was commenced in 12-week-old *mdx* mice in order to model the restoration of an internally deleted dystrophin protein in muscle with established pathology. Using highly sensitive and robust *in situ* functional assays (20–23), we have defined the relationship between levels of dystrophin restoration and improvements in muscle strength and resistance to eccentric contraction-induced muscle damage.

Results

Acute delivery of Pip6a-PMO protects muscle from eccentric contraction-induced damage

To facilitate the effective delivery of PMO, we undertook a study to directly compare the efficacy of a range of cell-penetrating peptide conjugates, B-PMO (24,25), B-MSP-PMO (26,27), Pip6e-PMO (19) and PMO alone following a dose of 12.5 mg/kg via either an intravenous (IV) or subcutaneous (SC) administration route (Supplementary Material, Figs. S1 and S2). The B-peptide is arginine rich ($[RXRRBR]_2$), the muscle potency and bio-distribution of which was originally assessed in the EGFP-654 transgenic reporter mouse (28). The chimeric peptide B-MSP-PMO incorporates a muscle-specific heptapeptide (ASSLNIAXB) between the arginine rich B-peptide and the PMO. Its enhanced delivery to skeletal muscle was originally identified through the screening of a random phage display library (29). The PNA-PMO internalization peptide (Pip) series was originally derived from the parent peptide Penetratin (30). Sequential modifications have created highly efficacious PPMOs consisting of a central hydrophobic core flanked on either side by arginine rich sequences (19). Previous assessment of these peptide-PMO conjugates in the *mdx* mouse model has recently been reviewed (31). No detectable levels of either exon 23 skipping or dystrophin protein were observed in skeletal or cardiac muscle following SC delivery of any of the compounds. High levels of exon skipping and dystrophin restoration were observed in skeletal muscle following a single IV dose of the P-PMOs but cardiac activity was only detected following the use of the Pip-peptide conjugate. The formulation of the Pip-peptide in either physiological saline or 5% D-glucose prior to injection did not alter its activity following either administration route although formulation in a lipid emulsion (50% Intralipid®) abolished all activity (Supplementary Material, Figs. S1 and S2). Following preparation in saline and an IV administration, the efficacy in both skeletal and cardiac muscle was enhanced with the use of an alternative Pip-peptide derivative; Pip6a-PMO (Supplementary Material, Fig. S3) (19).

To evaluate the efficacy of Pip6a-PMO a systemic dose-escalation study was carried out. *Mdx* mice were administered with a single dose of Pip6a-PMO (3, 6, 9 or 12.5 mg/kg) at 12 weeks of age, untreated age-matched male *mdx* mice were used as controls, muscle function was evaluated 2 weeks later. Using an *in situ* muscle eccentric contraction protocol, we measured resistance to eccentric contraction-induced muscle damage between the treatment groups. The acute systemic dose-escalation study revealed mice receiving higher doses of Pip6a-PMO (9 and 12.5 mg/kg) had significant protection against eccentric contraction-induced muscle damage (from eccentric contraction number three) in the tibialis anterior (TA) muscle, with a final tetanic force loss of only 23.4 ± 10.6% (9 mg/kg) and 22.3 ± 10.5% (12.5 mg/kg) compared with baseline. In contrast, mice from the untreated and lower dose treatment groups showed a greater force loss by the end of the eccentric contraction protocol: untreated, 60.40 ± 5.41%, 3 mg/kg, 54 ± 3.6% and 6 mg/kg, 51 ± 2.1% (Fig. 1A). Force–frequency curves showed a slight, but significant improvement on specific isometric force production at 150 and 180 Hz in only the 12.5 mg/kg treated mice compared with untreated controls (Fig. 1B).

Homogeneous sarcolemmal dystrophin protein expression was seen throughout the TA muscle in 12.5 mg/kg treated mice, with the dystrophin positive myofibres becoming patchier as the dose was decreased (Fig. 2A). We next quantified dystrophin protein in the exercised TA muscles. Western blot analysis of

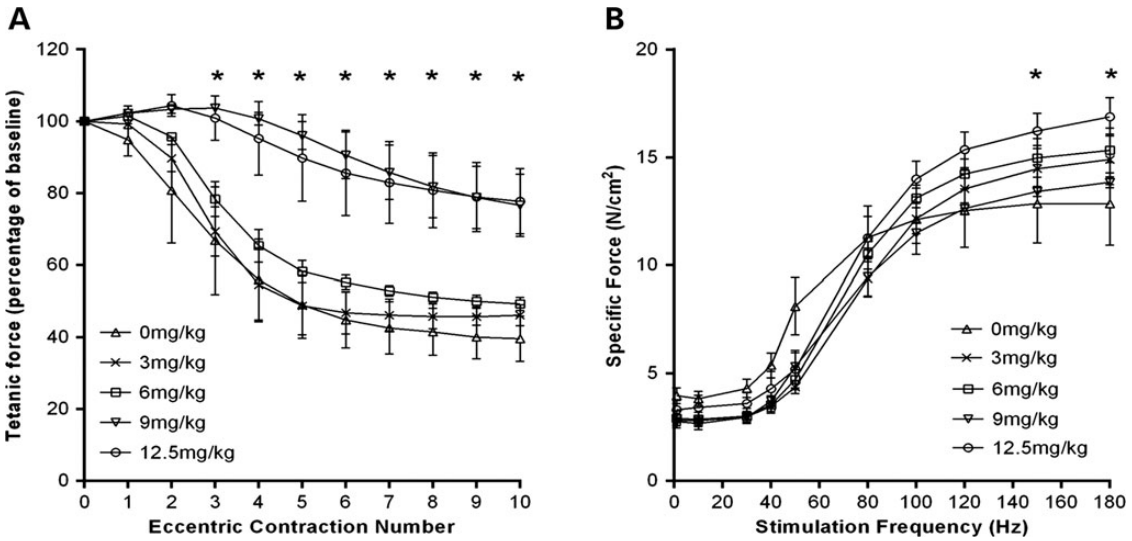

Figure 1. Acute delivery of Pip6a-PMO protects against muscle damage in *mdx* mice. Twelve-week-old male *mdx* mice received a single tail vein injection of Pip6a-PMO; 0 mg/kg, $n = 3$; 3 mg/kg, $n = 4$ ($n = 3$ for the eccentric protocol); 6 mg/kg, $n = 4$; 9 mg/kg, $n = 3$ or 12.5 mg/kg, $n = 4$. Muscle function was assessed 2 weeks later. (**A**) Using an eccentric contraction protocol (10% stretch of optimal muscle length), TA muscles were assessed for their resistance to eccentric contraction-induced muscle damage. Each tetanic force is expressed as a percentage of the baseline force produced prior to the first eccentric contraction. *Mdx* mice treated with either 9 mg/kg or 12.5 mg/kg of Pip6a-PMO had significant protection against eccentric contraction-induced muscle damage from contraction number three. (**B**) Force–frequency curve showing specific isometric force between the treatment groups (N/cm^2). A significant improvement in force production was only noted in 12.5 mg/kg treated mice at the higher stimulation frequencies (150 and 180 Hz), compared with untreated control mice. Statistical analysis; two-way repeated-measure ANOVA with Tukey's *post-hoc* test, (*$P \leq 0.05$). Error bars represent SEM.

internally deleted dystrophin revealed 5–15% of wild-type dystrophin levels in 9 and 12.5 mg/kg treated mice (Fig. 2B). Internally deleted dystrophin protein was not detectable in mice given 3 or 6 mg/kg (data not shown). In addition, quantitative analysis of the exon 23 skipped dystrophin transcripts demonstrated a Pip6a-PMO mediated dose-dependent increase of skipped transcripts (Fig. 2C). A significant reduction in the circulating serum biomarker tissue inhibitor metalloproteinase 1 (TIMP-1) (untreated mice; 11 957.6 ± 3167.6 pg/mL – 12.5 mg/kg mice; 3496.3 ± 387.1 pg/mL) was also noted as the dose of Pip6a-PMO increased (Fig. 2D). A linear regression analysis revealed a significant positive correlation between the percentage of restored dystrophin protein relative to wild-type and protection against eccentric contraction-induced muscle damage ($R^2 = 0.8687$, $P < 0.001$) (Fig. 2E).

These data reveal that 15% of wild-type levels of internally deleted dystrophin induced by a single dose of P-PMO is sufficient to protect against eccentric contraction-induced muscle damage, yet not enough to substantially improve muscle strength. We next designed a chronic dosing regimen to assess if repetitive delivery could further improve physiological muscle function.

Pre-clinical optimization of repeated P-PMO delivery

To establish the optimal treatment interval during a P-PMO repeated dosing strategy, we profiled the activity of a single dose of 12.5 mg/kg Pip6a-PMO in 12-week-old *mdx* males over time (Supplementary Material, Fig. S5A). Levels of *Dmd* exon 23 exclusion were broadly similar between tissues with peak activity observed at 1 or 2 weeks post systemic injection (TA; 49 ± 7.3%, heart; 45 ± 7.9% and diaphragm 43 ± 4.4%) while activity was barely detected 4 weeks post injection (Fig. 3A–C). Highest levels of total dystrophin protein restoration (TA; 37 ± 6.7%, heart; 58 ± 14.9% and diaphragm; 50 ± 8% relative to wild-type mice) (Fig. 3D–F and Supplementary Material, Fig. S6A) and sarcolemmal-associated dystrophin (TA; 54 ± 10%, heart; 40 ± 1% and diaphragm; 51 ± 8%) (Fig. 3G–L and Supplementary Material, Fig. S6B) were detected 1 week post injection in the TA and 2 weeks post injection in the heart and diaphragm. In contrast to the rapid decline of cardiac dystrophin levels 4 weeks post injection, a more stable restoration profile was seen in the TA with high levels of dystrophin protein detected 12 weeks post injection.

Repeated delivery of Pip6a-PMO protects and strengthens muscle

To evaluate the effects of long-term dosing of P-PMO on muscle function we treated 12-week-old male *mdx* ($n = 7$) with 12.5 mg/kg of Pip6a-PMO administered fortnightly for 20 weeks (Supplementary Material, Fig. S5B). Two weeks post treatment, we assessed resistance to eccentric contraction-induced muscle damage in treated and non-treated littermate control mice. Tibialis anterior muscles from Pip6a-PMO treated mice maintained maximal force production throughout the 10 eccentric contractions, similar to wild-type C57Bl/10 mice (Fig. 4A and Supplementary Material, Fig. S7A). In contrast, non-treated littermate controls exhibited a final 60 ± 3.9% drop in tetanic force production compared with the initial baseline force, with significantly lower tetanic forces compared with treated mice starting from eccentric contraction number two. Repeated delivery of Pip6a-PMO improved specific isometric force by 43% (19.32 ± 0.49 N/cm^2) compared with non-treated controls (13.55 ± 0.79 N/cm^2) (Fig. 4B and Supplementary Material, Fig. S7B). Homogeneous sarcolemmal dystrophin expression was observed throughout the whole of the TA muscle, with western blot analysis showing an average 50% restoration of internally deleted dystrophin protein relative to wild-type (Fig. 4C and D and Supplementary Material, Fig. S8A). Importantly, linear regression analysis revealed a positive correlation between maximal specific isometric force and the percentage of internally deleted dystrophin protein relative to wild-type ($R^2 = 0.8134$), a finding not previously reported in treated *mdx* mice (Fig. 4E).

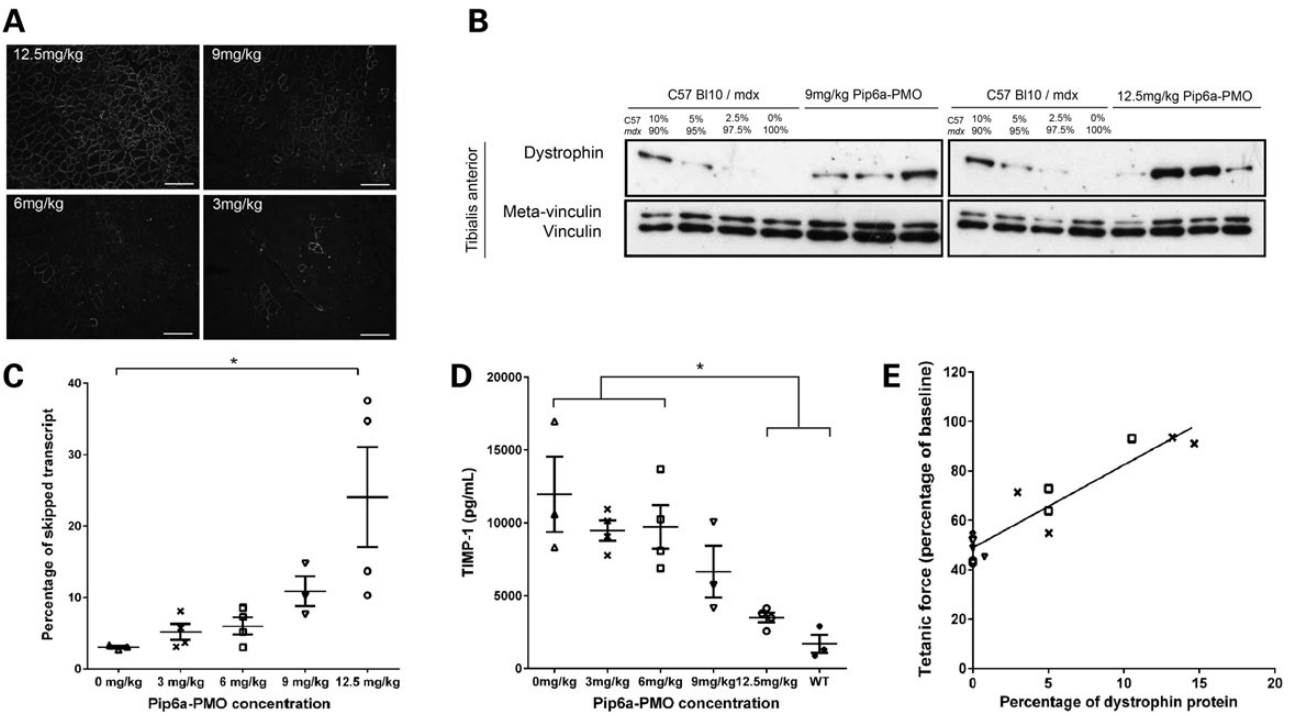

Figure 2. Acute delivery of Pip6a-PMO in *mdx* mice. Twelve-week-old male *mdx* mice received a single tail vein injection of Pip6a-PMO; 0 mg/kg, $n = 3$; 3 mg/kg, $n = 4$; 6 mg/kg, $n = 4$; 9 mg/kg, $n = 3$ or 12.5 mg/kg, $n = 4$. Muscle function was assessed 2 weeks later. (**A**) Immunohistochemistry confirmed homogenous sarcolemmal dystrophin expression throughout the TA muscle in mice treated with 12.5 mg/kg of Pip6a-PMO. The number of dystrophin positive fibres dramatically reduced in a dose-related response. Scale bar, 100 µm. (**B**) Western blot analysis of dystrophin protein 2 weeks after a single systemic Pip6a-PMO injection (9 mg/kg or 12.5 mg/kg). Analysis of internally deleted dystrophin revealed 5–15% of wild-type dystrophin expression levels in TA muscles of Pip6a-PMO treated *mdx* mice. Dystrophin protein was not detected in 6 mg/kg and 3 mg/kg treated mice (data not shown). (**C**) Reverse transcriptase–quantitative PCR (RT–qPCR) showing the percentage of exon skipping in TA muscles of Pip6a-PMO treated mice. We observed a significant increase in the percentage of dystrophin-skipped transcript in 12.5 mg/kg Pip6a-PMO treated mice compared with untreated controls. Kruskal–Wallis analysis with Dunn's *post-hoc* test, $n = 3/4$, $^*P \leq 0.05$. Error bars represent SEM. (**D**) Serum TIMP-1 expression in Pip6a-PMO treated mice. A significant reduction in circulating TIMP-1 protein in 12.5 mg/kg treated mice compared with 6 mg/kg and 3 mg/kg and untreated mice was noted. Statistical analysis; one-way ANOVA with Tukey's *post-hoc* test, ($^*P \leq 0.05$). Error bars represent SEM. (**E**) Linear regression analysis showing a positive correlation between resistance to eccentric contraction-induced muscle damage and dystrophin protein expression ($R^2 = 0.8687$, $P < 0.001$). Symbols represent: open triangles, 0 mg/kg; cross symbols, 3 mg/kg; open square, 6 mg/kg; inverted triangles, 9 mg/kg; open circle, 12.5 mg/kg.

Repeated delivery of Pip6a-PMO reduces muscle pathology

In light of the significant improvement in muscle function, we assessed whether chronic Pip6a-PMO treatment reduced muscle pathology. Localization of the dystrophin-associated protein complex (DAPC) proteins, beta-dystroglycan and recruitment of neuronal nitric oxide synthase (nNOS) was confirmed in TA muscles of Pip6a-PMO-treated mice (Supplementary Material, Fig. S8B). In addition, partial and/or complete normalization of circulating miR-206, miR-133a and miR-1 as well as TIMP-1 biomarkers was observed following repeated delivery (Supplementary Material, Fig. S9A–D). Interestingly, no significant difference in serum matrix metalloproteinase (MMP9) levels was noted between treated and untreated mice (Supplementary Material, Fig. S9E). Next, we assessed whether repeated treatment reduced muscle pathology by analysing myofibre size variation. A reduction in myofibre size variation, in particular the number of myofibres ≤40 µm and ≥70 µm was observed in TA muscles of Pip6a-PMO treated mice, indicating a drop in small regenerating myofibres and/or fibre splitting as well as decreased compensatory myofibre hypertrophy (Fig. 5A and B). Assessment of the diaphragm confirmed uniform dystrophin expression in all treated mice, as well as a reduction in fibrosis and inflammatory cell infiltration (Fig. 5C–H).

Discussion

Antisense oligonucleotide mediated splice modification is currently the most promising therapeutic intervention for DMD, as demonstrated in recent clinical trials (3,4). A major challenge facing the successful transition of this therapy to the clinic is to define the relationship between levels of genetic manipulation required for clinically relevant functional improvements. Despite a wealth of preclinical and clinical research, it is not yet known what levels of dystrophin restoration are needed within an established dystrophic environment to successfully modify disease progression (10,11,13,14,32).

In order to model the restoration of dystrophin in muscle with pre-existing pathology, we treated 12-week-old male *mdx* mice with P-PMO targeting the splicing of exon 23. To identify the optimal conditions for systemic dystrophin restoration, we initially compared delivery routes and formulations of a variety of P-PMO compounds. Prosensa initiated clinical trials utilizing a subcutaneous administration regimen with 2′-O-methyl AOs following pre-clinical studies demonstrating lower levels of AO detected in plasma, kidney and liver compared with an IV administration route potentially reducing any organ toxicity (4,33). We therefore investigated the potential of this delivery route for three leading classes of peptide-PMO conjugates (B-PMO, B-MSP-PMO and Pip6e-PMO) alongside PMO alone by directly comparing their

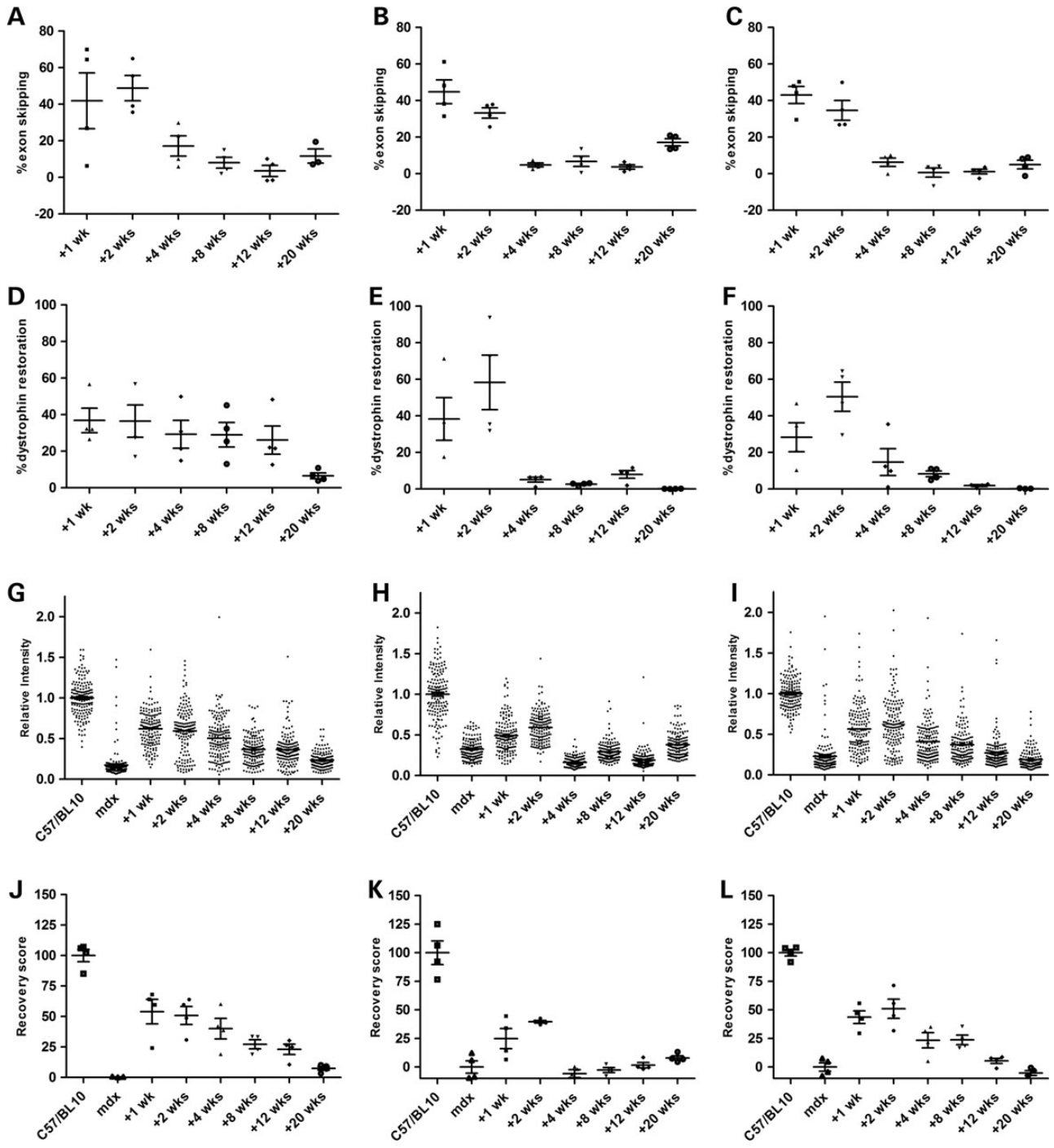

Figure 3. Tissue-specific profiling of exon skipping and dystrophin restoration following Pip6a-PMO administration. Twelve-week-old male *mdx* mice were treated with a single 12.5 mg/kg intravenous dose of Pip6a-PMO. Tissues were harvested 1, 2, 4, 8, 12 and 20 weeks post injection ($n = 4$). Data are shown from the TA (**A**, **D**, **G** and **J**), the heart (**B**, **E**, **H** and **K**) and the diaphragm (**C**, **F**, **I** and **L**). (A–C) Reverse transcriptase–quantitative PCR was performed to determine *Dmd* exon 23 exclusion. (D–F) Total dystrophin protein restoration was assessed by western blot using an infrared detection system. (G–I) Sarcolemmal-associated dystrophin expression was assessed by immunostaining; sarcolemmal intensity measurements quantified dystrophin relative to laminin-$\alpha 2$ and normalised to C57Bl/10; mean intensity values were used to generate a percentage recovery score (0%; untreated *mdx*, 100%; C57Bl/10) (J–L). Wks; weeks.

efficacy following either SC or IV administration. High levels of exon skipping and dystrophin restoration were observed in skeletal muscle following IV administration of the P-PMOs however, as expected, cardiac activity was restricted to the use of the Pip-peptide conjugate (19). Further improvements in efficacy were not detected following the preparation of P-PMO complexes in a variety of formulations. Following further refinement of the Pip-peptide-PMO sequence, Pip6a-PMO was selected for further use (19).

We then went on to assess the effects of restoring dystrophin levels on muscle pathology, as well as evaluating improvements in muscle functional using robust and reproducible *in situ* protocols

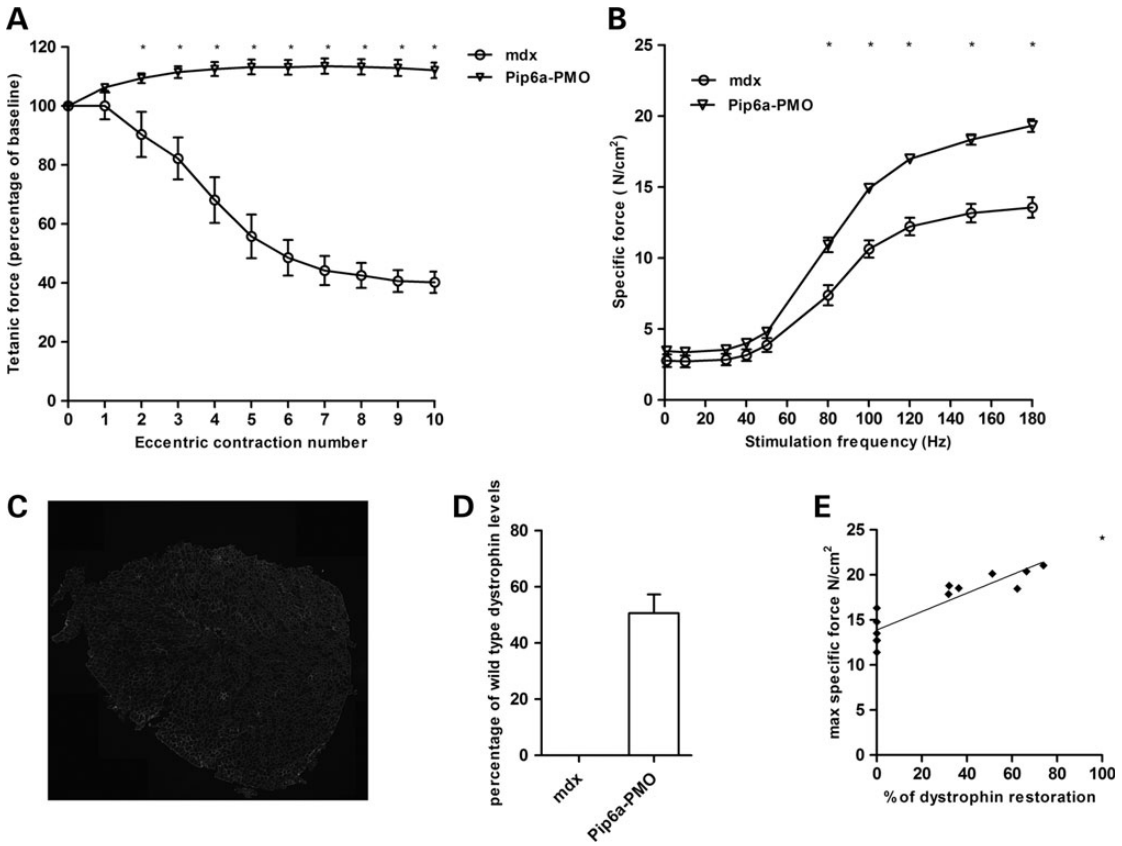

Figure 4. Chronic delivery of Pip6a-PMO restores muscle function in *mdx* mice. Twelve-week-old male *mdx* mice received 10 fortnightly tail vein injections of 12.5 mg/kg Pip6a-PMO. Muscle function was measured 2 weeks after the last tail vein injection. (**A**) TA muscles were assessed for their resistance to eccentric contraction-induced muscle damage (10% stretch of optimal muscle length). Each tetanic force is expressed as a percentage of the baseline force produced prior to the first eccentric contraction. Tetanic force was maintained throughout the protocol in Pip6a-PMO treated mice. In contrast, untreated *mdx* mice exhibited a 60 ± 3.9% drop in force compared with baseline, with a significant force drop starting from eccentric contraction number two. (**B**) Force–frequency graph of TA muscles from Pip6a-PMO treated *mdx* mice showing a significant improvement in specific force (N/cm^2) when stimulated between 80 and 180 Hz compared with untreated littermate controls. (**C**) Immunohistochemistry confirmed dystrophin expression was homogeneous throughout the muscle in treated mice. (**D**) Western blot analysis of total dystrophin protein 2 weeks after the last systemic Pip6a-PMO injection. On average, 50% of dystrophin levels (relative to wild-type) were restored in TA muscles of Pip6a-PMO treated *mdx* mice. (**E**) Linear regression analysis showing a positive correlation between maximal specific force and dystrophin protein expression ($R^2 = 0.8134$). The extrapolated data point highlights that 100% dystrophin levels yields a specific force of 24.1 N/cm^2, a maximal specific force value that is similar to wild-type C57B/l10 mice. Statistical analysis; two-way repeated-measures ANOVA with Tukey's *post-hoc* test, $n = 6$–7/group, $^*P \leq 0.05$. Error bar represents SEM.

to measure two independent parameters; muscle strength and resistance to contraction-induced muscle damage (34–37).

We performed an acute dose-escalation study to investigate whether a single administration of Pip6a-PMO was able to induce any detectable improvement in muscle physiology. Dystrophin restoration was only detectable by western blot following the 9 and 12.5 mg/kg doses. While positive sarcolemmal dystrophin staining was also detected in all treatment groups; a homogenous pattern of sarcolemmal dystrophin restoration was only observed following an acute injection of 12.5 mg/kg. Consistent with a previous study, biomarker analysis of circulating TIMP-1 showed a dose-dependent reduction, suggesting the protein to be a suitable marker for assessing treatment efficacy in the *mdx* mouse model (32).

The highest administered doses (12.5 and 9 mg/kg) were able to provide protection against eccentric contraction-induced muscle damage. *In situ* muscle physiology data also revealed a positive correlation between dystrophin restoration levels and protection against eccentric contraction-induced muscle damage. While we have previously reported a positive correlation following intramuscular injection of PMO (37), these data are the first to show almost complete protection against muscle damage following low level dystrophin restoration (~15%) with a single P-PMO intravenous injection. Sharp *et al.* (37) observed similar levels of muscle protection against eccentric contraction-induced muscle damage, with internally deleted dystrophin levels reaching 73% that of wild-type dystrophin levels. However, protein expression was only noted in ~65% of the total myofibres in the TA. In comparison, our data suggest that restoration of a low level, yet homogeneous sarcolemmal pattern of dystrophin expression in an established environment, provides greater muscle protection against eccentric contraction-induced damage than higher levels of dystrophin unevenly distributed throughout the muscle (patchy expression).

Although previous studies have highlighted the pathological and functional benefits of low dystrophin levels in transgenic mice models and patient cohorts, these approaches addressed dystrophin levels required to prevent disease development. As pre-natal therapy is not applicable for DMD and muscle pathology is present prior to diagnosis, we used a treatment based study design. Our data show low levels of homogenously distributed sarcolemmal dystrophin expression are sufficient to protect

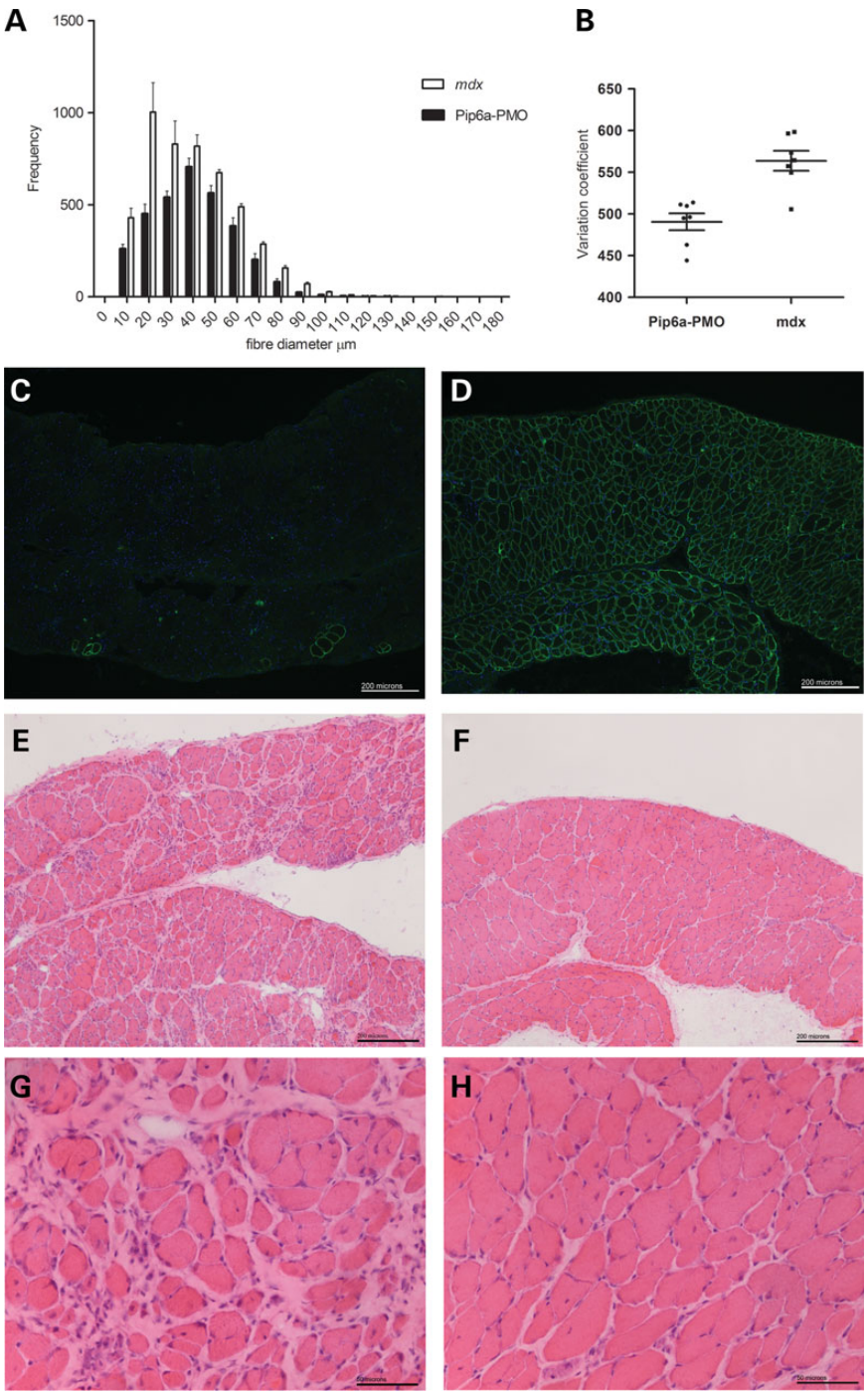

Figure 5. Reduced pathology in the TA and diaphragms of Pip6a-PMO treated mice. Using minimum Feret's diameter, the myofibre sizes in TA muscles from Pip6a-PMO treated and non-treated mice were assessed ($n = 7$). (**A**) A noticeable reduction in the number of myofibres under 40 μm and above 70 μm was observed in Pip6a-PMO treated mice indicating a reduction in small regenerating/fibre splitting and hypertrophic fibres, respectively. (**B**) Analysis of coefficient of variation confirmed a significant reduction in overall myofibre size variation in Pip6a-PMO treated mice. Unpaired *t*-test, $n = 7$/group, $P = 0.0005$. Immunohistological analysis of the diaphragm 2 weeks after the last tail vein injection of Pip6a-PMO. In contrast to untreated littermate control mice (**C**), homogenous sarcolemmal dystrophin expression was noted throughout the diaphragms of Pip6a-PMO treated mice (**D**). Histological analysis highlights a noticeable reduction in fibrosis and inflammatory infiltrate in Pip6a-PMO treated mice (**F** and **H**) compared with the untreated *mdx* mice (**E** and **G**).

against eccentric contraction muscle damage in the *mdx* mouse model even when a dystrophic environment has already been established. This work emphasizes the critical importance of selecting a delivery method for AOs that achieves uniform expression. Our interpretation of the dose dependency is that there is a critical level of dystrophin induction required to get a substantial level of dystrophin protein and this may be caused by the inhibition of dystrophin transcript translation by Mir31, proposed by (38). At the 3 and 6 mg/kg dose, the dystrophin transcript is effectively inhibited by high levels of Mir31. However, at 9 and 12.5 mg/kg, dystrophin expression is sufficient to escape Mir31 suppression of translation, and that the maturation of the muscle

then leads to a reduced level of Mir31 thus leading to greater levels of dystrophin than anticipated based on a simple dose–response relationship. However, we also note that this could be an artefact associated with a low number of mice in each group.

While it is important to establish the levels of dystrophin needed to prevent the muscle from undergoing further cycles of degeneration/regeneration and hence to slow down or prevent disease progression, only a slight significant improvement in specific force was noted in 12.5 mg/kg treated mice compared with untreated controls (at 150 and 180 Hz). However, due to the transient effect of AOs on splice modulation and the chronic nature of DMD, patients will require long-term repeated treatment. We therefore sought to investigate the same physiological parameters following repeated administration of Pip6a-PMO.

When designing a chronic dosing regimen, it is prudent to assess the persistence of *de novo* dystrophin expression following a single administration in order to establish the optimal treatment interval. Following a profiling study defining the activity of P-PMO over time, a 2-week treatment interval was selected in order to minimize the frequency of injection, yet ensure high levels of dystrophin restoration over time.

A repeated dosing strategy with Pip6a-PMO yielded ~50% dystrophin expression in TA muscle relative to wild-type and as expected, conferred complete protection against eccentric contraction-induced muscle damage. Interestingly, specific isometric force was improved by 43% compared with non-treated controls. In previous exon-skipping studies, increases in specific force have been ~20% (39,40). Here we demonstrate that a 20% increase is not in fact the upper limit to restoration of specific force (41). Upon extrapolation of these data, we noted that 100% dystrophin restoration would yield a specific force of 24.1 N/cm^2, a value strikingly similar to that obtained from wild-type mice, suggesting that the level of dystrophin restoration is a rate-limiting step for restoring muscle strength in the *mdx* mouse.

A recent study by Wu *et al.* (42) investigated the efficiency of exon skipping on disease progression in utrophin-dystrophin deficient mice. Their results demonstrated that the efficacy of AOs to moderate disease progression is highly dependent on level of muscle pathology at the time of intervention. Although our treatment regimens were commenced at a time when the *mdx* muscle had established pathology, 12-week-old *mdx* mice still retain a large amount of muscle mass, therefore while increases in specific force would translate clinically as improved muscle function in DMD patients, improvements would be highly moderated by the degree of muscle mass retention at the time of treatment.

In conjunction with the improved muscle function, a reduction in muscle pathology, in particular in the diaphragm, was noted in Pip6a-PMO-treated mice. The diaphragm was chosen for further investigation as it is severely affected in the *mdx* mouse (43). H&E analysis of the diaphragm highlighted a noticeable reduction in muscle fibrosis and cell infiltrate suggesting that chronic delivery of Pip6a-PMO may have halted/slowed down disease progression in this substantially affected muscle. Concomitant with improved muscle function and reduction in pathology, we observed partial and/or complete normalization of circulating miR-206, miR-133a and miR-1 suggesting that these may prove to be useful biomarkers of therapeutic effect in DMD (44,45). While published data (46) has shown MMP-9 to be a reliable marker for assessing disease progression in DMD patients (and not TIMP-1), our findings show TIMP-1, but not MMP9, is a sensitive marker of treatment effects in mice. Similar findings have also been shown in (32).

In conclusion, this is the first study to gain in depth understanding of the minimum levels of dystrophin needed to ameliorate muscle pathology in the *mdx* model once a dystrophic environment has been established. Our data have shown for the first time that homogeneous sarcolemmal expression of internally deleted dystrophin protein in dystrophic muscle amounting to ~15% of wild-type levels is sufficient to protect muscle against exercise-induced damage. Eccentric exercise is the most damaging form of muscle activity and maintenance of force in treated dystrophic muscle implies a prevention of further activity induced damage; thus suggesting a minimum of 15% restoration of dystrophin relative to wild-type is sufficient to halt the progressive muscle function decline. Discovery of a minimum dystrophin threshold will be of great value to the design of further clinical studies; however, here we also demonstrate that this level is insufficient to fully normalize muscle function, since improvements in muscle strength are proportional to the amount of dystrophin restored. Therefore, it is critically important to continue development of improved delivery systems for AOs in order to maximize dystrophin expression and hence the clinical efficacy of this therapeutic approach.

Materials and Methods

Study design

We sought to optimize splice modulation induced dystrophin restoration in the *mdx* mouse model using peptide conjugated-PMO. We used this approach to assess the levels of dystrophin needed to confer functional changes in a dystrophic muscle environment. Treatment of the *mdx* mouse model was commenced in 12-week-old males. P-PMO administration optimization experiments (route, peptide selection, P-PMO formulation) were assessed at 14 weeks of age following a single administration of 12.5 mg/kg ($n = 4$). The duration of exon skipping and dystrophin restoration was assessed at various time points following treatment ($n = 4$). Functional studies were performed on two cohorts of mice following either an acute ($n = 3$–4 per dose) or chronic treatment ($n = 6$–7) regimen with a randomized block design where mice from the same litter were randomly assigned to the different treatment groups. Researchers investigating muscle physiology, TIMP-1 levels, fibre sizes and microRNA levels were blinded as to whether the mouse had received P-PMO.

P-PMO synthesis and preparation

Pip6a peptide (Ac-RXRRBRRXRYQFLIRXRBRXRB-OH, with X = aminohexanoic acid and B = β-alanine) was synthesized by standard 9-fluorenylmethoxy carbonyl (Fmoc) chemistry, using a Liberty Peptide Synthesizer (CEM) on 100 μmol scale (19). Other peptides were synthesized similarly and the sequences are as previously described (19,26). The N-terminus of the peptide was acetylated with acetic anhydride before cleavage from the solid support using trifluoroacetic acid (TFA), 3,6-dioxa-1,8-octanedithiol (DODt), H_2O, triisopropylsilane (TIPS) in a ratio of (94%:2.5%:2.5%1%) (10 ml) for 3 h at room temperature. Excess TFA was removed and the crude peptide was isolated following precipitation with ice-cold diethyl ether. The peptide purified to >90% purity by standard reverse phase HPLC.

PMO (5′-GGCCAAACCTCGGCTTACCTGAAAT-3′) was purchased from Gene Tools, LLC (Philomath, OR, USA). Pip6a (2.5 molar excess over the PMO) was conjugated to the secondary amine at the 3′ end of the PMO through the C-terminal carboxyl group of the peptide following activation of this group with 2-(1H-benzotriazole-1yl)-1,1,3,3-tetramethyluronium hexafluorophosphate (HBTU) and 1-hydroxybenzotriazole (HOBt) in 1-methyl-

2-pyrrolidinone (NMP) and diisopropylethylamine (DIEA) using a HBTU:HOBt:DIEA (2.3:2.0:2.3) molar excess over the peptide. This mixture was added to a solution of PMO (10 mM) in DMSO (Dimethyl sulfoxide) and heated at 37°C for 2 h, after which time it was diluted with a 4-fold excess of water and purified on a cation exchange chromatography column (Resource S 6 ml column, GE Healthcare) using 25 mM sodium phosphate buffer (pH 7.2) containing 25% acetonitrile. 1 M sodium chloride was used to elute the conjugate from the column at a flow rate of 6 ml min^{-1}. The removal of excess salts from the Pip6a-PMO conjugate was afforded through the filtration of the fractions collected after ion exchange using an Amicon® ultra-15 3 K centrifugal filter device. The conjugate was lyophilized and analysed by MALDI-TOF. The conjugates were dissolved in sterile water and filtered through a 0.22 μm cellulose acetate membrane before use. The concentration of Pip6a-PMO was determined by the molar absorption of the conjugates at 265 nm in 0.1 N HCl (Hydrogen Chloride). Overall yields were 35–40% based on PMO.

Systemic administration of Pip6a-PMO

Experiments were conducted under Home Office Project Licence authorisation following institutional ethical review. All C57BL/10 and *mdx* mice were housed in a minimal disease facility, the environment was temperature controlled with a 12-h light-dark cycle. All animals received commercial rodent chow and water *ad libitum*. When anaesthetized, mice were induced with 5% isoflurane mixed with pure oxygen gas and maintained on 2% isoflurane. For route optimization studies, 12-week-old male *mdx* mice were anaesthetized prior to a single tail vein injection of 12.5 mg/kg with either PMO (M_r: 8413 g/mol), B-PMO (M_r:10 257 g/mol), B-MSP-PMO (M_r:11 027 g/mol) or Pip6e-PMO (M_r: 11 220 g/mol) in 160 μl of saline. These mice were compared with those given a SC injection of 12.5 mg/kg with either PMO, B-PMO, B-MSP-PMO or Pip6e-PMO in 300 μl of saline. To assess whether the formulation of P-PMO prior to injection affected its efficacy, 12-week-old male *mdx* mice were anaesthetized prior to a single tail vein injection of 12.5 mg/kg Pip6e-PMO formulated in either 5% D-glucose, physiological saline or intralipid (equivalent of 10% fat emulsion). To select the most efficacious P-PMO for further work, 12-week-old male *mdx* mice were anaesthetized prior to a single tail vein injection of 12.5 mg/kg with either Pip6a-PMO (M_r: 11 347 g/mol), Pip6b-PMO (M_r: 11 298 g/mol), Pip6e-PMO or Pip6f-PMO (M_r: 11 347 g/mol) in 160 μl of saline. Tissues were analysed 2 weeks post injection. For duration profiling of P-PMO over time, 12-week-old male *mdx* mice were restrained prior to a single tail vein injection of 12.5 mg/kg of Pip6a-PMO. For the acute dose escalation delivery, 12-week-old male *mdx* mice were anaesthetized prior to a single tail vein injection with either 3, 6, 9 or 12.5 mg/kg of Pip6a-PMO in 160 μl of saline. For chronic treatment, 12-week-old male *mdx* mice were anaesthetized prior to each tail vein injection of Pip6a-PMO (12.5 mg/kg) in 160 μl of saline. In total, 10 systemic injections of Pip6a-PMO (12.5 mg/kg) were given at 2-week intervals. Littermate mice were used as untreated controls. Two weeks after the last Pip6a-PMO injection, muscle function was assessed using the right TA muscle. Mice were surgically prepared and analysed as previously described (22,37).

Briefly, once surgically prepared optimal muscle length (Lo) was determined by increasing muscle length until the maximal twitch force was achieved. Next, to measure the force–frequency relationship, TA muscles were stimulated at different frequencies, delivered 1 min apart (1, 10, 30, 40, 50, 80, 100, 120, 150 and 180 Hz). Maximal isometric force (Po) was determined from the plateau of the force–frequency curve. Muscle fibre cross-sectional area (CSA in cm^2) was determined as previously described (22) and specific isometric force (N/cm^2) was calculated by dividing the absolute force (N) at each stimulation frequency by TA muscle physiological cross-sectional area.

To prevent muscle fatigue, a 5-min rest period was allowed before the initiation of the eccentric contraction protocol. The TA muscle was stimulated at 120 Hz for 500 ms before lengthening the muscle by 10% of the Lo at a velocity of 0.5 Lo s-1 for a further 200 ms, once the stimulation had ended the Lo returned at a rate of –0.5 Lo s-1. Between each contraction a 2-min rest period was permitted to avoid muscle fatigue. A total of 10 eccentric contractions were performed on each mouse. After each eccentric contraction, the maximum isometric force was measured and expressed as a percentage of the initial maximum isometric force achieved at the start of the protocol, prior to the first eccentric contraction. To measure circulating biomarkers, blood was collected via cardiac puncture (using a 23G needle) immediately after the eccentric contraction protocol. After cervical dislocation, TA muscles were removed and immediately weighed prior to snap-freezing in isopentane pre-chilled in liquid nitrogen. Statistical analysis for the force–frequency and eccentric contraction studies was measured by a repeated measure two-way ANOVA followed by a Tukey's *post-hoc* comparison. Statistical significance was defined as a value of $P < 0.05$.

Immunohistochemistry

To assess the duration of dystrophin restoration following a single administration, 8 μm transverse sections of TA, diaphragm and cardiac tissue were cut and mounted on slides. Intervening sections were collected and used for exon skipping and western blot analysis. Muscle pathology was assessed with Haemotoxylin and Eosin (H&E); staining protocol was carried out as previously described (22). Dystrophin and laminin protein expression was assessed simultaneously on unfixed sections with a double staining protocol using the polyclonal anti-dystrophin antibody (1:2500, 15 277 Abcam) and the monoclonal anti-laminin α2 antibody (1:1000, L0663 Sigma) (40). All primary antibodies were detected using species-appropriate fluorescently labelled secondary antibodies (1:500, Invitrogen). Once mounted, images were captured with a DM IRB Leica upright microscope (Zeiss monochrome camera) and AxioVision Rel. 4.8 software.

To evaluate dystrophin expression following acute dose escalation and chronic administration, 10 μm transverse sections were cut at 300 μm intervals throughout the exercised TA muscles with serial sections mounted on glass slides. Thirty intervening sections were collected and used for western blot and RT–qPCR analysis. Dystrophin protein expression was assessed on unfixed sections using the polyclonal anti-dystrophin antibody (1:800, 15 277, Abcam). Restoration of DAPC was evaluated with the monoclonal beta-dystroglycan (1:250, clone 8D5, a gift from Louise Anderson) and rabbit polyclonal nNOS antibodies (1:50, clone R20, Santacruz). All primary antibodies were detected using species-appropriate fluorescently labelled secondary antibodies (Invitrogen, 1:500) and nuclei were counterstained with Hoechst 33 342 (Invitrogen, 1:2000). Once mounted, all images were captured with the DM4000 Leica upright fluorescent microscope (Zeiss monochrome camera) and analysed using the AxioVision Rel. 4.8 software.

Immunohistological intensity measurements

Quantitative measurements of sarcolemma dystrophin restoration were performed as previously described (47). In brief, four random images were taken from four sections of TA, diaphragm

and heart from each treated animal. Using ImagePro software (MediaCybernetics), the intensity of laminin-α2 and dystrophin staining was recorded across 10 regions of sarcolemma within each image. These values were used to calculate recovery scores following treatment (http://www.treat-nmd.eu/downloads/file/sops/dmd/MDX/DMD_M.1.1_001.pdf).

Myofibre size analysis

Unfixed 10 µm TA sections were immunostained for the basement membrane proteoglycan, Perlecan (1:5000, Millipore) as previously described (37). Images were captured on a Leica DM4000 bright field microscope and a composite image of a whole TA section was created using Photoshop CS4. To avoid innate muscle variation all images were taken at the mid-belly of the TA muscle. Using a semi-automated programme (Leica QWin, macro developed by Dr Andrew Hibbert), minimum Feret's diameter was analysed (48), values were plotted in a frequency histogram and the coefficient of variation was calculated to assess fibre size variation [(Standard deviation/mean) × 1000]. Statistical significance on the coefficient variation was assessed using an unpaired *T*-test, $n = 7$. Statistical significance was defined as a value of $P < 0.05$.

Western blot analysis

To assess the duration of dystrophin restoration following a single administration, 8 µm transverse TA cryosections were lysed in buffer [75 mmol/l Tris–HCl (pH 6.5), 10% sodium dodecyl sulphate, 5% 2-mercaptoethanol and protease inhibitors] prior to centrifuging at 13 000 rpm (Heraeus, #3325B) for 10 min. Supernatant was collected and heated at 100°C for 3 min and fractionated on a 3–8% Tris–Acetate gel as previously described (19). Proteins were transferred and probed with monoclonal anti-dystrophin (1:200, NCL-DYS1, Novocastra) and anti-vinculin (loading control, 1:100 000, hVIN-1, Sigma) antibodies as previously described (37). Secondary antibody IRDye 800CW goat anti-mouse was used at a dilution of 1:20 000 (LiCOR). Fluorescence was detected and quantified using the Odyssey imaging system. Dystrophin expression was quantified using the dystrophin to vinculin ratio versus dystrophin expression level standards on each gel. To assess dystrophin expression in the TA muscle following acute dose escalation and chronic administration, 30 10 µm transverse TA cryosections were solubilized in RIPA buffer (50 mmol/l Tris–HCl (pH 8), 150 mM sodium chloride, 1% NP40, 0.5% sodium deoxycholate, 0.1% sodium dodecyl sulfate and protease inhibitors) for 10 min on ice prior to centrifuging at 13 000 rpm (Heraeus, #3325B) for 10 min at 4°C. Supernatant was collected and a small volume solubilized in 10% sodium dodecyl sulfate sample buffer, boiled for 3 min and fractionated on a 6% polyacrylamide gel, as previously described, with ∼7.5 µg/well (11,49). Proteins were transferred and probed with anti-dystrophin and anti-vinculin antibodies (discussed earlier). Secondary antibody goat anti-mouse IgG conjugated to horseradish peroxidase was used at a dilution of 1:100 000 (Biorad). Antibodies were detected by enhanced chemiluminescence (ECL Prime; Amersham Biosciences). The blots were exposed to X-ray film and developed using an automatic X-ray film processor (Processor X-ograph Imaging Systems). Densitometric quantification of band intensity was measured using Image J software. Loading levels and exposure times were empirically tested to be in the linear range aided by simultaneously scanning of an optical density control strip (Stouffer industries, Inc.). Dystrophin expression was quantitated using the dystrophin to vinculin ratio versus dystrophin expression level standards on each gel. Standard curves for a variety of dystrophin expression levels with a constant level of vinculin expression and total protein were generated by mixing different percentages of *mdx* and wild-type muscle homogenates and these were shown to be linear across the range from 2.5 to 80% wild-type dystrophin expression levels (Supplementary Material, Fig. S4, $R^2 = 0.98$). Sample aliquots were prepared and used for subsequent western blots. Three pre-defined standards were loaded onto each gel, values were plotted and used to determine dystrophin levels for the TA samples within treated and control animals. As our pre-defined standards were within a linear range, the line of best fit was extrapolated to calculate any of the values that were above the highest standard curve on any given gel.

RT–PCR analysis of Dmd Exon 23 skipping

In order to assess the degree of exon skipping following route and formulation studies in *mdx* mice, 400 ng of total RNA was used as a template in a 50 µl RT–PCR using the GeneAmp RNA PCR kit (Applied Biosystems). RT–PCR of the dystrophin transcript was performed under the following conditions; 95°C for 20 s, 58°C for 60 s and 72°C for 120 s for 30 cycles using the following primers: DysEx20Fo (5′–CAGAATTCTGCCAATTGCTGAG) and DysEx26Ro (5′–TTCTTCAGCTTGTGTCATCC). Two microlitres of this reaction was used as a template for nested amplification using Amplitaq Gold (Applied Biosystems) under the following conditions; 95°C for 20 s, 58°C for 60 s and 72°C for 120 s for 22 cycles using the following primers: DysEx20Fi (5′-CCCAGTCTACCACCCTATCAGAGC) and DysEx26Ri (5′-CCTGCCTTTAAGGCTTCCTT). PCR products were analysed on 2% agarose gels.

RT–qPCR analysis of Dmd Exon 23 skipping

To assess the percentage of exon skipping following the acute dose escalation study of Pip6a-PMO, RNA was extracted from TA muscles using Trizol (Invitrogen, Paisley, UK) according to manufacturer's instructions. One microgram of RNA was reverse transcribed using the RTnanoscript kit (PrimerDesign, UK) according to the manufacturer's instructions. qPCR was performed with Precision SYBR green mastermix (PrimerDesign) using 25 ng cDNA template. Primers were designed to amplify regions spanning Exons 1–3 (total dystrophin), Exons 22–23 (unskipped dystrophin), or spanning the novel splice junction of Exons 22:24, and Exon 25 (skipped dystrophin), and used the following sequences: Dys exon 1F (5′-GTGGGAAGAAGTAGAGGACTGTT-3′), Dys exon 3R (5′-AGGTCTAGGAGGCGT TTT CC-3′), Dys exon 22F (5′-GGAGGAGAGACTCGGGAAAT-3′), Dys exon 23R (5′-GTGC CC CT CAATCTCTTCAA-3′), Dys exon 22/24F (5′-CTCGGGAAATTACA GAATCACATA-3′), Dys exon 25R (5′-TCTGCCCACCTTCATTAACA-3′). Levels of respective transcripts were determined by calibration to standard curves prepared using known transcript quantities, and skipping percentages derived by [skip]/[skip+unskip]. Comparison of these values to [skip]/[total] gave a strong correlation ($R^2 = 0.99$) suggesting that [skip+unskip] was an accurate representative of the transcript population (non-canonical skipping which would not be detected by this method was very low or absent).

To investigate the duration of exon skipping following a single P-PMO administration, RNA was extracted from muscle sections using Trizol. One microgram of RNA was reverse transcribed using the High Capacity cDNA RT Kit (Applied Biosystems, Warrington, UK) according to manufacturer's instructions. qPCR analysis was performed using 25 ng cDNA template and amplified with Taqman Gene Expression Master Mix (Applied Biosystems, Warrington, UK) on a StepOne Plus Thermocycler

(Applied Biosystems, Warrington, UK). Levels of *Dmd* exon 23 skipping were determined by multiplex qPCR of FAM-labelled primers spanning Exon 20–21 (Assay Mm.PT.47.9564450, Integrated DNA Technologies, Leuven, Belgium) and HEX-labelled primers spanning Exon 23–24 (Mm.PT.47.7668824, Integrated DNA Technologies, Leuven, Belgium). The percentage of *Dmd* transcripts containing exon 23 was determined by normalizing exon 23–24 amplification levels to exon 20–21 levels.

Serum protein and microRNA biomarkers

Blood samples collected via cardiac puncture were left to clot for 10 min at room temperature prior to centrifuging at 1800 g for 10 min at 4°C, serum was removed and stored at −80°C. Levels of TIMP-1 and MMP9 expression were analysed using the mouse TIMP-1 (MTM100) and MMP9 (MMPT90) immunoassays from R&D systems. Serum samples were diluted 1:10 (TIMP-1) or 1:50 (MMP9) in respective assay calibrator diluents and analysed in duplicates according to manufacturer's instructions. Sera from age-matched wild-type C57Bl/10 female mice were used as controls. We have previously confirmed there is no significant difference in MMP-9 and TIMP-1 levels between male and female mice (data not shown). Statistical analysis was measured using either a Kruskal–Wallis test followed by a Dunn's *post-hoc* test or a one-way ANOVA with Tukey's *post-hoc* test. Statistical significance was defined as a value of $P < 0.05$. For microRNA analysis, RNA was extracted from 50 µl of serum using TRIzol LS (Invitrogen, Paisley, UK) as according to manufacturer's instructions. A synthetic miRNA, cel-miR-39, was added as a normalization control at the organic extraction phase. miRNAs of interest were reverse transcribed using Taqman miRNA Reverse Transcription Kit (Applied Biosystems, Warrington, UK) and quantified by small RNA TaqMan RT–qPCR (Applied Biosystems, Warrington, UK) with levels normalized to the spike-in cel-miR-39 and endogenous miR-223. All primer/probe assays were purchased from Applied Biosystems (Warrington, UK).

Supplementary Material

Supplementary Material is available at *HMG* online.

Conflict of Interest statement. M.J.W., M.J.G. and C.B. are inventors on a filed patent on identification of cell-penetrating peptides and conjugates of a cell-penetrating peptide and a cargo molecule filed jointly by the Medical Research Council and the University of Oxford. D.J.W. is a member of the Scientific Advisory Board for Akashi Therapeutics, a firm developing non-antisense based treatments for DMD.

Funding

This work was supported by grants from the Association Française contre les Myopathies (C.G., G.M., K.W., T.C. and L.O.; programme number 14784), the Muscular Dystrophy Campaign (C.B.; programme number RA4/858), the Duchenne Research Fund (J.H.), the Medical Research Council (S.H.; programme number G0900887) and the Wellcome Trust (R.T.). Work in the laboratory of M.J.G. was supported by the Medical Research Council (MRC programme number U105178803).

References

1. Manzur, A.Y., Kinali, M. and Muntoni, F. (2008) Update on the management of Duchenne muscular dystrophy. *Arch. Dis. Child.*, **93**, 986–990.
2. Muntoni, F. and Wood, M.J. (2011) Targeting RNA to treat neuromuscular disease. *Nat. Rev. Drug Discov.*, **10**, 621–637.
3. Cirak, S., Arechavala-Gomeza, V., Guglieri, M., Feng, L., Torelli, S., Anthony, K., Abbs, S., Garralda, M.E., Bourke, J., Wells, D.J. *et al.* (2011) Exon skipping and dystrophin restoration in patients with Duchenne muscular dystrophy after systemic phosphorodiamidate morpholino oligomer treatment: an open-label, phase 2, dose-escalation study. *Lancet*, **378**, 595–605.
4. Goemans, N.M., Tulinius, M., van den Akker, J.T., Burm, B.E., Ekhart, P.F., Heuvelmans, N., Holling, T., Janson, A.A., Platenburg, G.J., Sipkens, J.A. *et al.* (2011) Systemic administration of PRO051 in Duchenne's muscular dystrophy. *N. Engl. J. Med.*, **364**, 1513–1522.
5. Kinali, M., Arechavala-Gomeza, V., Feng, L., Cirak, S., Hunt, D., Adkin, C., Guglieri, M., Ashton, E., Abbs, S., Nihoyannopoulos, P. *et al.* (2009) Local restoration of dystrophin expression with the morpholino oligomer AVI-4658 in Duchenne muscular dystrophy: a single-blind, placebo-controlled, dose-escalation, proof-of-concept study. *Lancet Neurol.*, **8**, 918–928.
6. van Deutekom, J.C., Janson, A.A., Ginjaar, I.B., Frankhuizen, W.S., Aartsma-Rus, A., Bremmer-Bout, M., den Dunnen, J.T., Koop, K., van der Kooi, A.J., Goemans, N.M. *et al.* (2007) Local dystrophin restoration with antisense oligonucleotide PRO051. N. Engl.J. Med., **357**, 2677–2686.
7. Lu, Q.L., Cirak, S. and Partridge, T. (2014) What Can We Learn From Clinical Trials of Exon Skipping for DMD? *Mol. Ther. Nucleic Acids.*, **3**, e152.
8. Neri, M., Torelli, S., Brown, S., Ugo, I., Sabatelli, P., Merlini, L., Spitali, P., Rimessi, P., Gualandi, F., Sewry, C. *et al.* (2007) Dystrophin levels as low as 30% are sufficient to avoid muscular dystrophy in the human. *Neuromuscul. Disord.*, **17**, 913–918.
9. Anthony, K., Cirak, S., Torelli, S., Tasca, G., Feng, L., Arechavala-Gomeza, V., Armaroli, A., Guglieri, M., Straathof, C.S., Verschuuren, J.J. *et al.* (2011) Dystrophin quantification and clinical correlations in Becker muscular dystrophy: implications for clinical trials. *Brain*, **134**, 3547–3559.
10. Phelps, S.F., Hauser, M.A., Cole, N.M., Rafael, J.A., Hinkle, R.T., Faulkner, J.A. and Chamberlain, J.S. (1995) Expression of full length and truncated dystrophin mini-genes in transgenic mdx mice. *Hum. Mol. Genet.*, **4**, 1251–1258.
11. Wells, D.J., Wells, K.E., Asante, E.A., Turner, G., Sunada, Y., Campbell, K.P., Walsh, F.S. and Dickson, G. (1995) Expression of human full-length and minidystrophin in transgenic *mdx* mice: implications for gene therapy of Duchenne muscular dystrophy. *Hum. Mol. Genet.*, **4**, 1245–1250.
12. Li, D., Yue, Y. and Duan, D. (2008) Preservation of muscle force in Mdx3cv mice correlates with low-level expression of a near full-length dystrophin protein. *Am. J. Pathol.*, **172**, 1332–1341.
13. Li, D., Yue, Y. and Duan, D. (2010) Marginal level dystrophin expression improves clinical outcome in a strain of dystrophin/utrophin double knockout mice. *PLoS One*, **5**, e15286.
14. van Putten, M., Hulsker, M., Nadarajah, V.D., van Heiningen, S.H., van Huizen, E., van Iterson, M., Admiraal, P., Messemaker, T., den Dunnen, J.T., t Hoen, P.A.C. *et al.* (2012) The effects of low levels of dystrophin on mouse muscle function and pathology. *PLoS One*, **7**, e31937.
15. Bulfield, G., Siller, W.G., Wight, P.A. and Moore, K.J. (1984) X chromosome-linked muscular dystrophy (mdx) in the mouse. *Proc. Natl Acad. Sci. U S A.*, **81**, 1189–1192.
16. Coulton, G.R., Morgan, J.E., Partridge, T.A. and Sloper, J.C. (1988) The mdx mouse skeletal muscle myopathy: I. A histological, morphometric and biochemical investigation. *Neuropathol. Appl. Neurobiol.*, **14**, 53–70.

17. Dangain, J. and Vrbova, G. (1984) Muscle development in mdx mutant mice. *Muscle Nerve*, **7**, 700–704.
18. Tanabe, Y., Esaki, K. and Nomura, T. (1986) Skeletal muscle pathology in X chromosome-linked muscular dystrophy (mdx) mouse. *Acta. Neuropathol.*, **69**, 91–95.
19. Betts, C., Saleh, A.F., Arzumanov, A.A., Hammond, S.M., Godfrey, C., Coursindel, T., Gait, M.J. and Wood, M.J. (2012) Pip6-PMO, A New Generation of Peptide-oligonucleotide Conjugates With Improved Cardiac Exon Skipping Activity for DMD Treatment. *Mol. Ther. Nucleic Acids.*, **1**, e38.
20. Foster, H., Sharp, P.S., Athanasopoulos, T., Trollet, C., Graham, I.R., Foster, K., Wells, D.J. and Dickson, G. (2008) Codon and mRNA sequence optimization of microdystrophin transgenes improves expression and physiological outcome in dystrophic mdx mice following AAV2/8 gene transfer. *Mol. Ther.*, **16**, 1825–1832.
21. Miller, G., Moore, C.J., Terry, R., La Riviere, T., Mitchell, A., Piggott, R., Dear, T.N., Wells, D.J. and Winder, S.J. (2012) Preventing phosphorylation of dystroglycan ameliorates the dystrophic phenotype in mdx mouse. *Hum. Mol. Genet.*, **21**, 4508–4520.
22. Terry, R.L., Kaneb, H.M. and Wells, D.J. (2014) Poloxomer 188 has a deleterious effect on dystrophic skeletal muscle function. *PLoS One*, **9**, e91221.
23. Whitmore, C., Fernandez-Fuente, M., Booler, H., Parr, C., Kavishwar, M., Ashraf, A., Lacey, E., Kim, J., Terry, R., Ackroyd, M.R. *et al.* (2014) The transgenic expression of LARGE exacerbates the muscle phenotype of dystroglycanopathy mice. *Hum. Mol. Genet.*, **23**, 1842–1855.
24. Crisp, A., Yin, H., Goyenvalle, A., Betts, C., Moulton, H.M., Seow, Y., Babbs, A., Merritt, T., Saleh, A.F., Gait, M.J. *et al.* (2011) Diaphragm rescue alone prevents heart dysfunction in dystrophic mice. *Hum. Mol. Genet.*, **20**, 413–421.
25. Yin, H., Moulton, H.M., Seow, Y., Boyd, C., Boutilier, J., Iverson, P. and Wood, M.J. (2008) Cell-penetrating peptide-conjugated antisense oligonucleotides restore systemic muscle and cardiac dystrophin expression and function. *Hum. Mol. Genet.*, **17**, 3909–3918.
26. Yin, H., Moulton, H.M., Betts, C., Seow, Y., Boutilier, J., Iverson, P.L. and Wood, M.J. (2009) A fusion peptide directs enhanced systemic dystrophin exon skipping and functional restoration in dystrophin-deficient mdx mice. *Hum. Mol. Genet.*, **18**, 4405–4414.
27. Yin, H., Moulton, H.M., Betts, C., Merritt, T., Seow, Y., Ashraf, S., Wang, Q., Boutilier, J. and Wood, M.J. (2010) Functional rescue of dystrophin-deficient mdx mice by a chimeric peptide-PMO. *Mol. Ther.*, **18**, 1822–1829.
28. Jearawiriyapaisarn, N., Moulton, H.M., Buckley, B., Roberts, J., Sazani, P., Fucharoen, S., Iversen, P.L. and Kole, R. (2008) Sustained dystrophin expression induced by peptide-conjugated morpholino oligomers in the muscles of mdx mice. *Mol. Ther.*, **16**, 1624–1629.
29. Samoylova, T.I. and Smith, B.F. (1999) Elucidation of muscle-binding peptides by phage display screening. *Muscle Nerve*, **22**, 460–466.
30. Perez, F., Joliot, A., Bloch-Gallego, E., Zahraoui, A., Triller, A. and Prochiantz, A. (1992) Antennapedia homeobox as a signal for the cellular internalization and nuclear addressing of a small exogenous peptide. *J. Cell. Sci.*, **102**, 717–722.
31. Boisguerin, P., Deshayes, S., Gait, M.J., O'Donovan, L., Godfrey, C., Betts, C.A., Wood, M.J. and Lebleu, B. (2015) Delivery of therapeutic oligonucleotides with cell penetrating peptides. *Adv. Drug. Deliv. Rev.*, **4**, 00019–00018.
32. van Putten, M., Hulsker, M., Young, C., Nadarajah, V.D., Heemskerk, H., van der Weerd, L., t Hoen, P.A., van Ommen, G.J. and Aartsma-Rus, A.M. (2013) Low dystrophin levels increase survival and improve muscle pathology and function in dystrophin/utrophin double-knockout mice. *FASEB J.*, **27**, 2484–2495.
33. Heemskerk, H., de Winter, C., van Kuik, P., Heuvelmans, N., Sabatelli, P., Rimessi, P., Braghetta, P., van Ommen, G.J., de Kimpe, S., Ferlini, A. *et al.* (2010) Preclinical PK and PD studies on 2′-O-methyl-phosphorothioate RNA antisense oligonucleotides in the mdx mouse model. *Mol. Ther.*, **18**, 1210–1217.
34. Chan, S., Head, S.I. and Morley, J.W. (2007) Branched fibers in dystrophic mdx muscle are associated with a loss of force following lengthening contractions. *Am. J. Physiol. Cell. Physiol.*, **293**, 985–992.
35. Dellorusso, C., Crawford, R.W., Chamberlain, J.S. and Brooks, S.V. (2001) Tibialis anterior muscles in mdx mice are highly susceptible to contraction-induced injury. *J. Muscle. Res. Cell. Motil.*, **22**, 467–475.
36. DelloRusso, C., Scott, J.M., Hartigan-O'Connor, D., Salvatori, G., Barjot, C., Robinson, A.S., Crawford, R.W., Brooks, S.V. and Chamberlain, J.S. (2002) Functional correction of adult mdx mouse muscle using gutted adenoviral vectors expressing full-length dystrophin. *Proc. Natl Acad. Sci. USA*, **99**, 12979–12984.
37. Sharp, P.S., Bye-a-Jee, H. and Wells, D.J. (2011) Physiological characterization of muscle strength with variable levels of dystrophin restoration in mdx mice following local antisense therapy. *Mol. Ther.*, **19**, 165–171.
38. Cacchiarelli, D., Incitti, T., Martone, J., Cesana, M., Cazzella, V., Santini, T., Sthandier, O. and Bozzoni, I. (2011) miR-31 modulates dystrophin expression: new implications for Duchenne muscular dystrophy therapy. *EMBO Rep.*, **12**, 136–141.
39. Aoki, Y., Nakamura, A., Yokota, T., Saito, T., Okazawa, H., Nagata, T. and Takeda, S. (2010) In-frame dystrophin following exon 51-skipping improves muscle pathology and function in the exon 52-deficient mdx mouse. *Mol. Ther.*, **18**, 1995–2005.
40. Malerba, A., Sharp, P.S., Graham, I.R., Arechavala-Gomeza, V., Foster, K., Muntoni, F., Wells, D.J. and Dickson, G. (2011) Chronic systemic therapy with low-dose morpholino oligomers ameliorates the pathology and normalizes locomotor behavior in mdx mice. *Mol. Ther.*, **19**, 345–354.
41. Heier, C.R., Damsker, J.M., Yu, Q., Dillingham, B.C., Huynh, T., Van der Meulen, J.H., Sali, A., Miller, B.K., Phadke, A., Scheffer, L. *et al.* (2013) VBP15, a novel anti-inflammatory and membrane-stabilizer, improves muscular dystrophy without side effects. *EMBO Mol. Med.*, **5**, 1569–1585.
42. Wu, B., Cloer, C., Lu, P., Milazi, S., Shaban, M., Shah, S.N., Marston-Poe, L., Moulton, H.M. and Lu, Q.L. (2014) Exon skipping restores dystrophin expression, but fails to prevent disease progression in later stage dystrophic dko mice. *Gene Ther.*, **21**, 785–793.
43. Stedman, H.H., Sweeney, H.L., Shrager, J.B., Maguire, H.C., Panettieri, R.A., Petrof, B., Narusawa, M., Leferovich, J.M., Sladky, J.T. and Kelly, A.M. (1991) The mdx mouse diaphragm reproduces the degenerative changes of Duchenne muscular dystrophy. *Nature*, **352**, 536–539.
44. Roberts, T.C., Blomberg, K.E., McClorey, G., El Andaloussi, S., Godfrey, C., Betts, C., Coursindel, T., Gait, M.J., Smith, C.I. and Wood, M.J. (2012) Expression analysis in multiple muscle groups and serum reveals complexity in the microRNA transcriptome of the mdx mouse with implications for therapy. *Mol. Ther. Nucleic Acids*, **1**, e39.

45. Zaharieva, I.T., Calissano, M., Scoto, M., Preston, M., Cirak, S., Feng, L., Collins, J., Kole, R., Guglieri, M., Straub, V. *et al.* (2013) Dystromirs as serum biomarkers for monitoring the disease severity in Duchenne muscular Dystrophy. *PLoS One*, **8**, e80263.
46. Nadarajah, V.D., van Putten, M., Chaouch, A., Garrood, P., Straub, V., Lochmuller, H., Ginjaar, H.B., Aartsma-Rus, A.M., van Ommen, G.J., den Dunnen, J.T. *et al.* (2011) Serum matrix metalloproteinase-9 (MMP-9) as a biomarker for monitoring disease progression in Duchenne muscular dystrophy (DMD). *Neuromuscul. Disord.*, **21**, 569–578.
47. Arechavala-Gomeza, V., Kinali, M., Feng, L., Brown, S.C., Sewry, C., Morgan, J.E. and Muntoni, F. (2010) Immunohistological intensity measurements as a tool to assess sarcolemma-associated protein expression. *Neuropathol. Appl. Neurobiol.*, **36**, 265–274.
48. Briguet, A., Courdier-Fruh, I., Foster, M., Meier, T. and Magyar, J.P. (2004) Histological parameters for the quantitative assessment of muscular dystrophy in the mdx-mouse. *Neuromuscul. Disord.*, **14**, 675–682.
49. Wells, D.J., Wells, K.E., Walsh, F.S., Davies, K.E., Goldspink, G., Love, D.R., Chan-Thomas, P., Dunckley, M.G., Piper, T. and Dickson, G. (1992) Human dystrophin expression corrects the myopathic phenotype in transgenic mdx mice. *Hum. Mol. Genet.*, **1**, 35–40.